Current spectra under varying stratification conditions in the central North Sea

Hans van Haren

Royal Netherlands Institute for Sea Research (NIOZ), P.O. Box 59, 1790 AB Den Burg (Texel), The Netherlands

Abstract

Given strongly different vertical stratification and not significantly different kinetic energy, 'internal wave' band spectral properties were studied using two 8-day representative sets of observations from the central North Sea in winter and summer. The observed similar spectral shape of the internal wave band was due to a combination of deterministic narrow band and intermittent signals. In addition to dominant tidal harmonics, 25% of total kinetic energy was found at inertial and non-linear inertial-tidal interaction frequencies in summer and about the same amount was found in broad-band response to atmospheric forcing in winter. The energy at the (seasonal) non-linear interaction frequencies was proportional to stratification, specifically, to near-inertial shear magnitude. In summer, motions at frequencies (σ) between $f < \sigma < 2.5$ cpd (cycles per day) appeared in low vertical mode, whilst the power $P(\sigma)$ of motions at $\sigma > 4 \pm 1$ cpd obeyed canonical internal wave scaling $P(\sigma) \sim C\sigma^{-2}$, provided the shear magnitude $|\mathbf{S}|$ was used instead of the buoyancy frequency N for the factor C. Motions at $2.5 < \sigma < 4 \pm 1$ cpd appeared as transition between the two regimes. In winter no inertial motions were observed.
© 2004 Elsevier B.V. All rights reserved.

Keywords: Spectra; Seasonal stratification; Central North Sea

1. Introduction

Between mid-spring and -autumn, shelf seas such as the central North Sea (Fig. 1) show enhanced vertically stable stratification in density, mainly due to vertical temperature differences (Fig. 2a, b). In theory, such stratification may support internal gravity waves in the internal wave frequency (σ) band (IWB) $f < \sigma < N$, $f \ll N$, where f denotes the local inertial frequency and N the buoyancy or stability frequency. When N varies slowly with time as with the seasons

one expects the frequency range of IWB to vary as well and also its energy level, because of the changing restoring force. This is expressed in the canonical internal wave kinetic energy spectrum scaling, which is given by $P(\sigma) \propto N\sigma^{-p}$, $1.5 < p < 2.5$ $f \ll \sigma \ll N$ (Garrett and Munk, 1972; henceforth GM). Such scaling is observed to within a factor of 2 in smoothed open ocean spectra (Fofonoff and Webster, 1971; GM), whilst its applicability for shelf seas is unknown.

Despite strong seasonal variations in stratification and atmospheric forcing, observed kinetic energy spectra between $f < \sigma < \sim 10$ cpd from mid-depth in the central North Sea appear similar in summer and winter (Fig. 2c). This apparent contrast with ('open

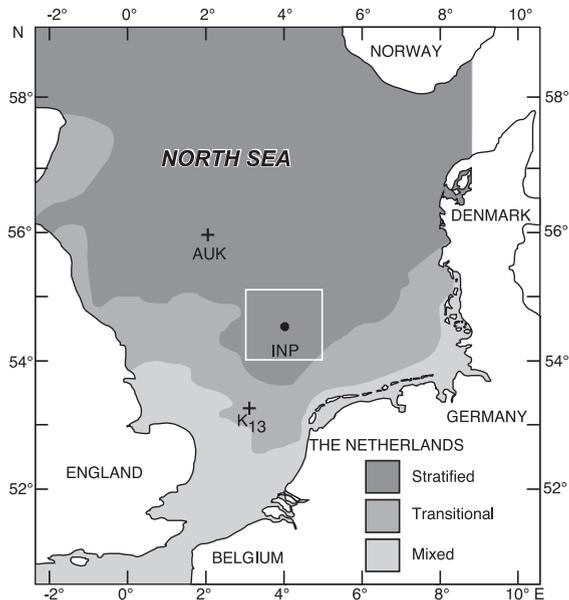*E-mail address:* hansvh@nioz.nl (H. van Haren).

Fig. 1. Map of the central North Sea showing the mooring site (INP; 54°25′ N, 04°02′ E) and two meteorological platforms K13 and AUK. Shading of summer stratification adapted from Pingree and Griffiths (1978).

ocean') GM either implies 'sufficient' stratification in the central North Sea or dominance of turbulence in the IWB in winter, or a lack of free internal waves in summer. Or, could the IWB be filled by non-internal wave motions as a result of typical shelf sea processes such as strong non-linearity and vertically varying transport of momentum due to varying viscosity? This question is raised for several reasons.

First, in contrast with the open ocean a shelf sea is conceptually modelled as a 2(3)-layer system with 'well-mixed' turbulent surface and bottom boundary layers and a thin, strongly stratified layer in between. (The original GM-model uses >10 vertical modes, whilst later versions ∼ 4 modes). In such a 2(3)-layer system internal waves appear predominantly in only two vertical modes, the barotropic mode with vertically uniform currents and the first baroclinic mode with horizontal current components in opposite direction above and below the stratification (LeBlond and Mysak, 1978). Although present-day sophisticated numerical models provide much more detailed insights than this conceptual model, the first order internal wave motions appear in first baroclinic mode predominantly (e.g. Davies and Xing, 2002).

Second, near-inertial motions *appear* predominantly in such first baroclinic mode, but observations and modelling by Millot and Crépon (1981) have shown that this vertical inertial current structure is not due to internal wave motions. Instead it is attributable to slab-layer motion by reduced viscosity in the stratification, the generation of barotropic motions partially counter-acting the near-surface slab-layer motion, matched through a coastal boundary condition.

Third, free internal tidal waves are largely absent in the central North Sea (Van Haren and Maas, 1987; Howarth, 1998). Ubiquitous tidal variability in temperature and current observations is mainly due to differential advection of horizontal gradients. Enhanced vertical tidal current differences across stratification are well explained in terms of Ekman dynamics using vertically varying viscosity (Maas and Van Haren, 1987).

Fourth, barotropic motions at semi-diurnal tidal and its non-linear higher harmonic frequencies are found in the same frequency range as internal waves, so that the frequency range of the IWB does not necessarily contain just free internal waves. Such barotropic motions are commonly found in shelf seas due to advection and bottom friction, see e.g. Dronkers (1964), Pingree and Maddock (1978), and several papers in Parker (1991).

Fifth, it has been suggested that in the presence of strong inertial motions enhanced energy is found at non-linear inertial-tidal interaction frequencies dominating the internal wave band energy levels (Mihaly et al., 1998; Van Haren et al., 1999, 2002).

In this paper, the focus is on spectral analysis of central North Sea currents at super-inertial frequencies, henceforth the IWB. A correspondence is sought between the IWB energy levels and varying stratification and forcing. In other words, for example, if $N \neq 0$ and $f < N$ in winter: how large must N be to support internal waves and how strong are non-internal wave motions within the IWB? In Section 2, we discuss some of the IWB properties typical for shelf seas. In Section 3 we describe site, data and methods. In Section 4, we discuss detailed observations of the IWB for a single site in the topographically featureless central North Sea and we compare these observations with independent observations of stratification. In Section 5, we discuss implications and estimates of
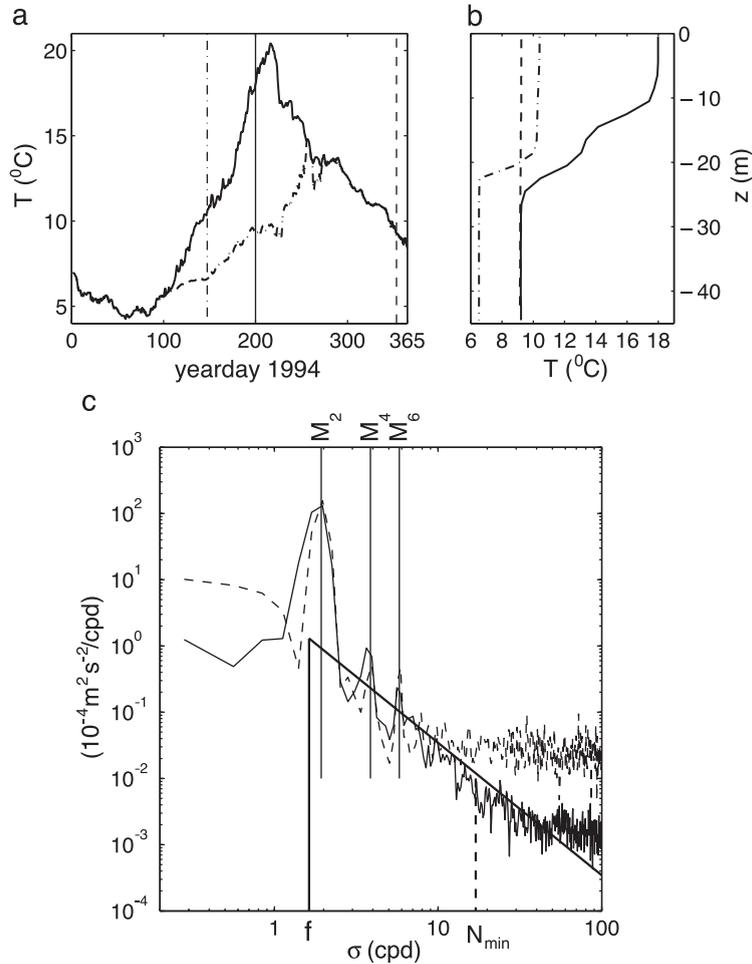
Fig. 2. (a) Surface (solid line) and bottom (dashed line) temperatures observed at INP (Fig. 1) as a function of time, which is given according to the convention that 1 January, 12.00 UTC equals yearday 0.5 (in 1994). (b) Profiles of temperature with depth observed at days 150 (dash-dotted line), 200 (solid line) and 355 (from CTD data; dashed line). (c) Spectra of 8 days of current observations from 17 m depth during summer (solid line) and winter (dashed line). The apparently enhanced noise level in the winter spectrum is due to surface wave aliasing (Van Haren, 2001). The number of degrees of freedom df ≈ 5 so that the effective bandwidth $(\Delta\sigma)_{eff} \approx 0.35$ cpd. A simple graphic showing σ^{-2} spectral decay is given by the solid line between the inertial frequency f and the buoyancy frequency N (the dashed line is at $N_{min} \approx 10f$, Eq. (3)). This graphic will be consistent in subsequent figures on spectra, for comparison.

the influence of the atmosphere on the IWB. Section 6 is a summary of conclusions.

2. Seasonal stratification in a shelf sea

2.1. Stability

Local static stability occurs when $N^2 > 0$, where the buoyancy frequency is defined as $N = N(z) = -g$ dln(ρ)/dz. In terms of observable static state distributions of temperature $T = T_0(z)$, salinity $s = s_0(z)$ (Gill, 1982; Pond and Pickard, 1986), and, in shelf seas, concentration density of suspended material C(z, t), N(z) reads,

$$N(z)^2 = g\left\{\alpha\left(\frac{dT_0}{dz} + \frac{\alpha T_0 g}{c_p}\right) - \beta\frac{ds_0}{dz} - \frac{1}{\rho}\frac{dC}{dz}\right\},$$

$$(1)$$

in which $\alpha = -\rho^{-1}\partial\rho/\partial T$ and $\beta = \rho^{-1}\partial\rho/\partial s$ denote expansion coefficients, g the acceleration of gravity and c_p the specific heat at constant pressure. Part of the second term on the right-hand side indicates the adiabatic lapse rate $\Gamma = \alpha T_0 g/c_p$. In a system without suspended material, with constant salinity and in thermal equilibrium, so that $T_0(z) = T_c$, density stratification remains statically stable because $\Gamma > 0$. For such a system with temperature varying between $4 < T_c < 20$ °C, buoyancy periods are $\tau_{Nc} = 2\pi[c_p/\alpha^2 T_c g^2]^{0.5} \approx 2.5–7$ h, all smaller than the mid-latitude inertial period $\tau_f \sim 15$ hours and yielding an IWB which is a quarter to half a decade wide,

$$N_c = \left(\frac{\alpha^2 T_c g^2}{c_p}\right)^{0.5} \approx 2.2 - 5.5f. \qquad (2)$$

In the entire water column in winter and in the frictional bottom boundary layer all year around, horizontal advection and resuspension of material by combined wave action, wind and tidal friction results in $\partial C/\partial z = 5\cdot10^{-5} - 10^{-3}$ kg m^{-4} (Van Raaphorst et

al., 1998). This provides 5–25f of N, with the largest values near the bottom where little thermal and haline stratification is found. Near the bottom $\partial C/\partial z$ may vary with the tidal period, being generated by friction. In spring and early summer as soon as weak thermal stratification occurs near the surface, sinking phytoplankton biomass values provide $\partial C/\partial z = 10^{-6}$ kg m^{-4} near the bottom (Gieskes and Kraay, 1984), adding 1f to N.

Considering the above, we estimate a minimum stratification, which is valid all year round in shelf seas, as

$$N_{min} \approx \overline{N}_c + 6f \approx 10f, \qquad for\ T \approx 10°C. \qquad (3)$$

We do not expect a void internal wave band causing a spectral gap, except under conditions of convective instability.

In summer, stratification becomes much larger due to heating by the sun ($N \gg N_{min}$; $N \approx 35N_{min} \approx 350f$ in Fig. 3). However, once stable stratification exists, internal dynamic de-stabilisation may occur. For example, inertial shear supported by
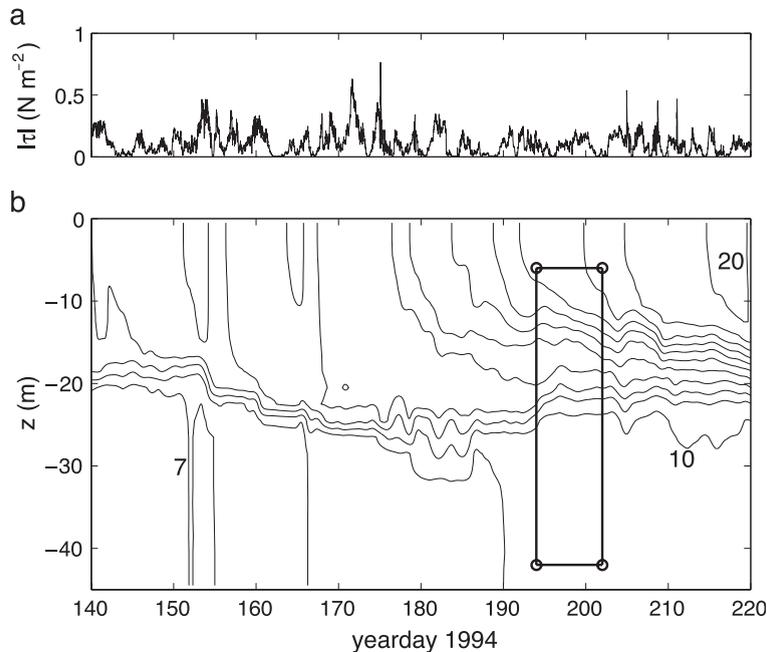

Fig. 3. Middle half of the period of seasonal stratification. (a) Wind stress magnitude $|\tau| = \rho_a Cd|\mathbf{W}|^2$, where $\mathbf{W}$ denotes the wind vector measured at platform K13, ρ_a the density of air and Cd a constant drag coefficient. (b) Temperature distribution indicated using daily-filtered isotherms (thin solid lines, drawn every 1 °C, between 7–20 °C). The solid (-o-) box indicates the (t, z) range of summertime ADCP measurements.

enhanced stratification may cause the occasional breaking of small-scale internal waves (Van Haren et al., 1999).

2.2. Suggestions for construction of the internal wave band

Atmospheric forcing occurs by wind stress and air pressure. We distinguish two different current responses to such forcing in a stratified sea, (1) baroclinic, narrow-band (relative extent in frequency $\Delta\sigma/\sigma \sim 0.1$) response at near-inertial frequencies $\sigma = (1+\varepsilon)f$, $\varepsilon \ll 1$ (Millot and Crépon, 1981), and (2) barotropic, broad-band response (extending well beyond IWB limits, Krauss, 1972; Gill, 1982). Current magnitudes are inversely proportional to their associated local vertical length scales, which are surface 'mixed layer' depth ($h \ll H$, under stratified conditions; Pollard and Millard, 1970; Pollard et al., 1973) and the water depth H. Implicitly, this associates near-inertial response with stratification. Total energy may be larger for broad-band response than for narrow-band response, considering the ratio of the two depths is only one order of magnitude ($h \gtrsim 0.1H$) in shelf seas. This contrasts with suggestions for omnipresent dominance of near-inertial response in the open ocean (Gill, 1982).

In the simplest linear model, broad-band response to wind stress (assuming flat response functions) for two different frequency bands reads,

$$|\langle \bar{\mathbf{u}} \rangle| = \frac{\rho_a \mathrm{Cd}}{\rho \mathrm{Hf}} |\bar{\mathbf{W}}|^2, \qquad \sigma \ll f$$

$$|\langle \mathbf{u}' \rangle| = \frac{\rho_a \mathrm{Cd}}{\rho \mathrm{H}\sigma} |\mathbf{W}'|^2, \qquad \sigma \gg f \tag{4}$$

where $\langle\ \rangle$ denotes vertical averaging, the overbar and prime denote low- and high-frequency parts of a signal, the latter including the internal wave band. Current and wind vectors are given by $\mathbf{u}$ and $\mathbf{W}$, respectively. $\mathrm{Cd} = 2 \times 10^{-3}$ is a drag coefficient at the surface, ρ_a is the density of air. Qualitatively, (4) corresponds with results by Krauss (1972), who found that wind stress generation dominated current response over most of the frequency-wave number plane in a stratified shelf sea (the Baltic).

A universal internal wave spectrum may be shaped internally by a saturation process (Munk, 1981), rather than through an external generation process. Hence, under sufficient stratified conditions in addition to direct atmospheric forcing, the narrow-band response near f may fill the spectrum by cascading energy through non-linear interactions. According to a simple interaction model (as for instance for shock waves by Platzman, 1964), the associated spectrum consists of sharp higher harmonics at all possible combination (sum and difference) frequencies of the fundamental motions.

3. Site, data and methods

During the Integrated North Sea Program (INP) we obtained data in the central North Sea (Fig. 1) to study the effects of diapycnal mixing on the distribution of phytoplankton. At this location $f = 1.185 \times 10^{-4}$ s^{-1} (1.63 cpd, cycles d^{-1}) so that the inertial period $\tau_f \approx 14.7$ h. The water depth H = 45 m and major topographic features were at least 50 km away. In winter, motions at semidiurnal tidal frequencies dominated horizontal currents whose amplitudes varied between 0.2–0.3 m s^{-1} (mainly neap-spring). The surface tidal current ellipse was nearly rectilinear with the major axis directed E-W (so that $u \gg v$).

Between November 1993 and February 1995, we deployed up to six moorings in a 600 by 600 m square area, effectively guarded by four large buoys. Besides instrumentation monitoring biological and chemical parameters, standard Aanderaa thermistor strings monitored temperature from surface to bottom, with thermistors at least every 2 m. Also throughout the 15-month period four-five mechanical NBA-current meters were located between 13–40 m depth. For 8 d in summer and one month in winter a 600 kHz RDI BB-ADCP (acoustic Doppler current profiler) resolved almost the entire water column in 0.5 m vertical increments. Because of this high vertical resolution we focus here on the ADCP data. These data were sampled once every 2.5 or 5 min, so that $\sigma_{\mathrm{Nyq}} \approx 100f$ which was sufficient to resolve $N_{\min}$, but not the buoyancy period observed in the main thermocline in summer. The instrumental accuracy was ~ 0.01 m s^{-1} per sample. From the one-month winter-data, a sub-sample of 8 d was

taken to match the length of the summer-data record. The winter subset was chosen to cover the same portion of the spring-neap cycle as in the summer-data and to be representative of wintertime atmospheric forcing. We sampled meteorological data continuously 150–200 km from the mooring site (Fig. 1). We performed Seabird SBE-911 CTD-sampling for hydrographic and calibration purposes every 3–4 weeks during mooring servicing cruises.

For temperature stratification, when $dT/dz > 0.1$ °C m^{-1}, salinity contributions to density variations were negligible. In winter, salinity contributed about 60–70% to density stratification. Using smoothed T-ρ relationships we inferred time-depth evolution of static stability from thermistor string data. CTD-temperature sensors had an accuracy of about 0.001 °C after careful calibration. The thermistor string sensors had an accuracy of only 0.05 °C after laboratory calibration supplementing the factory calibration and resolution of 0.025 °C. Assuming purely random errors, a one-week mean buoyancy frequency of $N \sim 6f$ (T = 10 °C) was measurable using thermistor string data.

Considering proper statistics (with sufficient degrees of freedom, $\nu \gg 10$ df), separation of closely spaced frequencies such as f and M_2 (lunar semidiurnal tidal frequency) required data records of several months. This allowed us to determine only long-term average properties. In this paper, the long-term (seasonal and longer) equilibrium was not the subject of study. We were interested in properties averaged over periods of typically a week to resolve narrow-band and broad-band response to in- and external forcing. As a compromise, near-raw spectra were presented for the lowest number of degrees of freedom (usually 3–5 'df'; *cf.* Fig. 2c). This was achieved by tapering the entire time series using a single cosine-bell shaped window or repeating that window once in a half-overlapping fashion. Ripples were strongly reduced and the effective bandwidth, $(\Delta\sigma)_{eff} \approx 0.2$–0.3 cpd for a week of data, was about twice the fundamental bandwidth.

We split current observations (U, V)(z, t) at each depth and for each time step into two parts. By definition, the vertically averaged parts $\langle U \rangle$, $\langle V \rangle$ contained 'barotropic' motions (driven by surface pressure gradient forces) and the remainder, the 'baroclinic' parts, contained internal waves *and* short-scale phase-locked motions. Using 0.5 m vertical depth resolution ADCP data we defined,

$$\langle U \rangle = \int_{-35}^{-10} U \ dz/25, \quad \text{barotropic current,}$$
$$u = U - \langle U \rangle, \quad\quad\quad\quad \text{baroclinic current,}$$

(5)

and similarly for the V-component. This process resolved typical vertical length scales of current shear $|\mathbf{S}| = ((\partial u/\partial z)^2 + (\partial v/\partial z)^2)^{0.5}$ across enhanced stratification. It also excluded most of the frictionally near-bottom ($-45 < z < -35$ m) and -surface ($-10 < z < 0$ m) layers in the averaging process (Maas and Van Haren, 1987). However, this averaging did not exclude modification of barotropic (tidal) currents by varying viscosity associated with stratification.

In frequency, we studied details of the IWB by splitting *baroclinic* currents into four parts, using sharp symmetric band-pass filters. We considered the 'total baroclinic internal wave' band ($2.5 < \sigma < 25$ cpd; indicated by the current amplitude '$\mathbf{U}_{iw}$'), which was composed of the 'fourth-diurnal' band ($2.5 < \sigma < 5$ cpd; '$\mathbf{U}_{iw}^{(4)}$'), the 'sixth-diurnal' band ($4.5 < \sigma < 10$ cpd; '$\mathbf{U}_{iw}^{(6)}$') which included N_c, and the 'high-frequency internal wave' band ($9 < \sigma < 25$ cpd; '$\mathbf{U}_{iw}^{(h)}$'), which included N_{min}. Within these bands we named specific frequency bands (such as 'inertial', 'semidiurnal tidal' and 'fourth-diurnal' bands) after their dominant constituent (f, M_2 and M_4, in this example), which were short hand for all frequencies in the effective bandwidth around the dominant constituents.

4. Observations

4.1. Stratification in winter

CTD observations during a day of relatively calm weather in December suggested that (3) holds for the lower half of the water column (Fig. 4a-c). Assuming $\partial C/\partial z = 0$, we observed static instability ($N < 0$) regularly in the upper half of the water column (Fig. 4b). During storms, bottom material was resuspended up to the surface layer (Fig. 4c). It was estimated that the minimum IWB_{min} ($f < \sigma < N_{min}$) was maintained throughout the water column, lasting ~ 5 days before material was settled and some remained suspended throughout the winter.
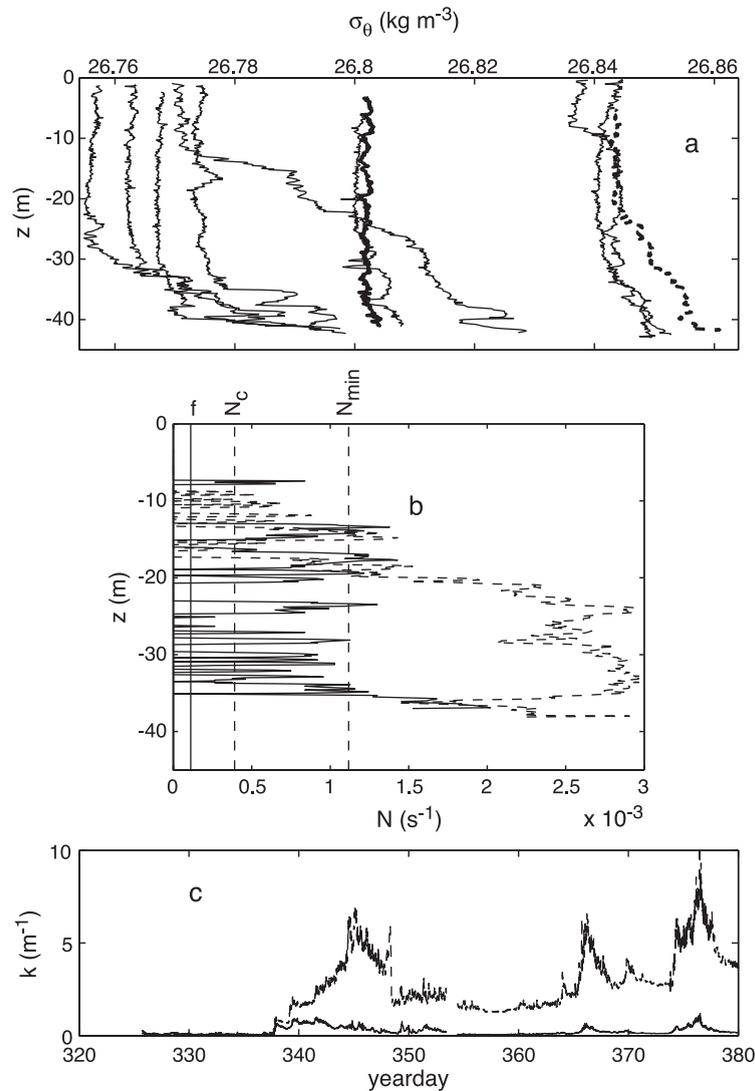
Fig. 4. Wintertime stability observations. (a) CTD profiles of density anomaly with depth observed close to the mooring between days 353.26 and 354.63, stations randomly distributed through time. (b) Profiles of stability frequency corresponding to the heavy solid (day 353.99) and dashed (354.14) profiles in a. Only in winter, is N determined by salinity for about two-thirds. N is computed as in (1) except for $\partial C/\partial z$ term, and smoothed by a triangular filter with 3.5 m half-width, so that data are available from $-38 < z < -5$ m. (c) Beam attenuation (k) observed using transmissometers at 15 (lower line) and 38 m depth (upper line). Winter calibration data were not available. For indication: in summer k in $m^{-1} \sim$ concentration in mg m^{-3}, around k = 1 m^{-1}. Time in yeardays, with 12.00 UTC on 1 January 1995 = day 365.5.

4.2. Kinetic energy spectra

Spectra (henceforth short hand for 'kinetic energy spectra') in summer and winter had equal total *and* equal tidal harmonic kinetic energy (Fig. 2c). We confirmed this by splitting currents into barotropic and baroclinic parts using (5).

4.2.1. Barotropic currents

Spectra of barotropic currents did not show gaps in the IWB. In that frequency range they were dominated at fundamental semidiurnal tidal (M_2), a single uneven (M_3) and a sequence of even higher harmonic (M_4, M_6,...) frequencies superposed on a non-zero continuum (Fig. 5a). This continuum ex-

tended to sub-inertial and super-N_{min} frequencies. In winter, this barotropic kinetic energy continuum was $3-10$ times larger than in summer. After removal of tidal harmonics it contained $\sim 25\%$ of the total barotropic kinetic energy. It seemed related to the wind stress, as the average variance of the latter was about 3 times higher in winter than in summer (Fig. 5b). This suggested a frequency independent transfer

function between wind stress and currents, in contrast with (4). (We used the first (frequency independent) equation of (4) to plot Fig. 5b, also for $\sigma > f$).

We did not verify quantification of coupling between wind stress and vertically averaged currents. We expected correlation between measurements at sites $150-200$ km apart would not be significant
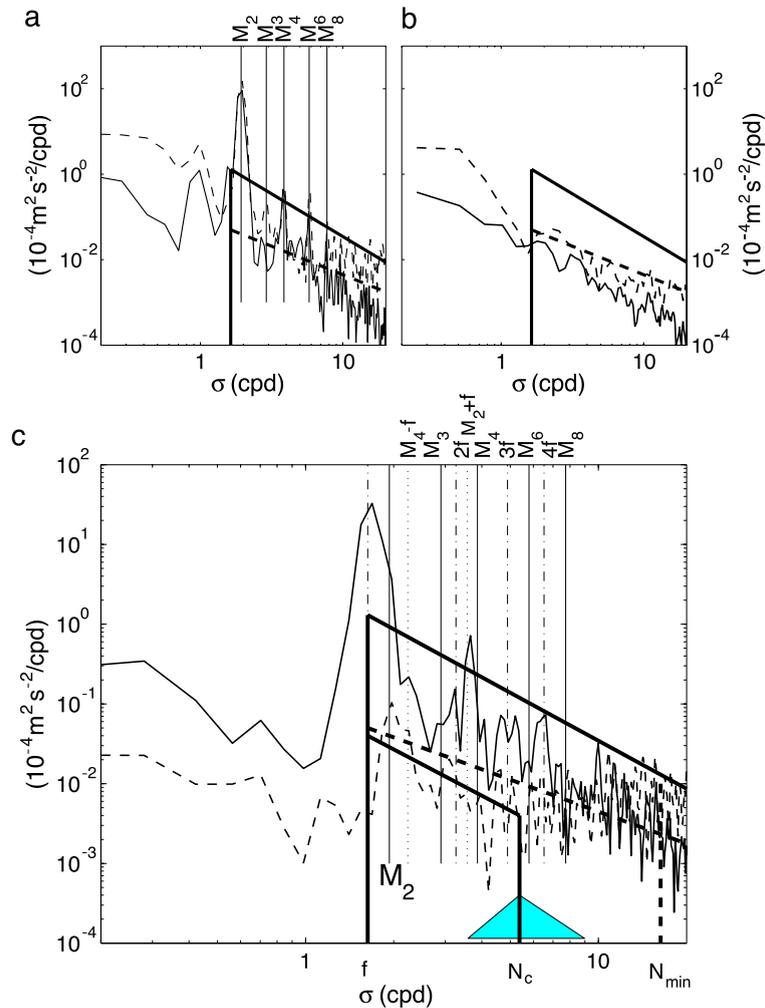

Fig. 5. (a) Near-raw spectra (df ≈ 3; $(\Delta\sigma)_{eff}$ ≈ 0.23 cpd) for *barotropic* currents (defined in (4) of 8 days of ADCP observations in summer (solid graph) and winter (dashed) as in Fig. 2c. In addition to the simple graphic indicating the σ^{-2} spectral decay the heavy dashed line indicates a σ^{-1} spectral slope, which is repeated in (b) and (c). (b) Spectra (df ≈ 5) of the scaled wind stress vector T = a W^2[sin(R), cos(R)], where the wind speed (W) and direction (R) have been measured at platform K13 (Fig. 1). The factor a = ρ_aCd/ρHf is kept constant here, for a simple transfer to kinetic energy (see text for explanation of symbols). (c) As in (a) but for the *baroclinic* currents at 17 m depth. The vertical distance between the two solid lines sloping like σ^{-2} equals 32, equal to the mean local shear ratio, and about half the local N ratio (Fig. 4b for wintertime N at 17 m). The triangular base around $\sigma = N_c = 3.3f$ indicates possible variability of N_c according to (2).

and this was indeed the case. We made no observations of pressure gradient (geostrophic balance). There was no vertically mean narrow-band near-inertial response to atmospheric forcing.

4.2.2. Baroclinic motions

In summer, baroclinic IWB kinetic energy showed levels that were $1-2$ decades larger than in winter (Fig. 5c), comprising about 25% of total kinetic energy. Most of the summertime baroclinic energy was at f with values about half a decade lower than at barotropic M_2. As a result, the level of the summertime IWB was equal to the wintertime barotropic 'wind stress' continuum. This winter barotropic continuum roughly showed a σ^{-1} spectral slope in the IWB, in contrast with the GM σ^{-2} internal wave spectral slope.

In winter, we found a σ^{-2}-slope in a mid-depth baroclinic spectrum only when we included energy at semidiurnal frequencies. This spectrum barely exceeded white noise levels and nevertheless its energy levels were 'just' one decade below those of the summertime baroclinic spectrum between M_4-f $< \sigma < 2$f. At these frequencies, a spectral depression was found with respect to the σ^{-2} slope, independent of the season. Similarly, baroclinic M_4, M_6, M_8 showed spectral *gaps*. In contrast, at inertial-tidal interaction frequencies like M_4-f, $M_2 + $f the summer/ winter kinetic energy ratio was ~ 100. The mean of this ratio was ~ 35, close to the ratio of summer- and winter-buoyancy frequencies, except in periods of convection.

Throughout the water column, the summertime baroclinic IWB spectral continuum fell off at a rate of σ^{-2}, whilst peaks at inertial-tidal frequencies showed a steeper slope, σ^{-3} (Fig. 6b). When scaled with the mean local buoyancy frequency (Fig. 6a), spectra collapsed to a mean level within a factor of 2 as in GM, but only when U_{iw} exceeded instrumental noise ($N > \sim 25$ cpd). In weaker stratified
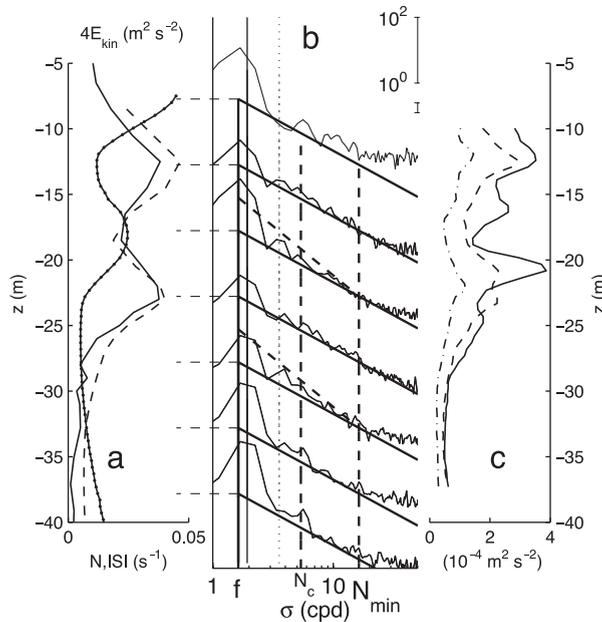

Fig. 6. IWB spectra between days $194-202$. (a) Rms buoyancy frequency (solid graph), current shear magnitude (dashed) and total kinetic energy for baroclinic currents (solid-dot graph; multiplied by a factor of four (see top) to match the scale at the bottom). (b) Spectra (df ≈ 10) scaled with |**S**| from a. for baroclinic currents at depths indicated by the horizontal dashed lines referring to the vertical scale in a. The vertical spectral scale is at the top (in 10^{-4} m^{2}s^{-2}/cpd), and each spectrum has been relatively offset by two decades. The thin vertical solid line is at M_2, the dotted line at $M_2 + $f. The sloping solid lines fall off as σ^{-2}, the sloping dashed lines at 17 and 27 m depth as σ^{-3}. (c) Profiles of kinetic energy with depth from band-pass filtered baroclinic currents $U_{iw}^{(4)}$ (solid graph), $U_{iw}^{(6)}$ (dashed) and $U_{iw}^{(h)}$ (dash-dotted).

parts ($z > -10$ m, $z < -25$ m) the spectrum flattened into white noise at $N \approx N_{min}$ rather than rolling off. Near the surface this noise was due to surface wave aliasing (Van Haren, 2001); near the bottom it was due to (tidal) mixing. At these depths, N^1-scaling appeared too large and scaling with N^n ($0.5 < n < 1$) or with $|S|^1$ seemed more appropriate (Fig. 6b). We noted that in weak stratification N was more difficult to measure than **S** and quantitative evidence on C(z) was lacking. However, associating a mean gradient Richardson number $Ri = N^2/|S|^2 \approx 1$ for strong stratification (Van Haren et al., 1999) and $Ri \approx 0.25$ in strongly turbulent boundary layers, $|S|^1 \approx Ri^{-0.5}N^1$-scaling.

4.2.3. Vertical structure of baroclinic IWB motions

The above confirmed CTD-observations that in the mean the central North Sea was always sufficiently stratified to support internal waves. However, not all of the IWB was attributable to free propagating internal waves, which we inferred from the vertical structure of average kinetic energy in different bands of IWB (Fig. 6a, c). Largest IWB motions near f appeared predominantly in low vertical standing mode (mode-1; Fig. 6a), alternating high amplitudes with large stratification at different depths. This was in agreement with the findings by Millot and Crépon (1981). Note that for $z < -25$ m motions at f were absent, probably due to bottom friction. In contrast, high frequency IWB motions $U_{iw}^{(h)}$ (Fig. 6c) showed strong association with stratification, implying, given the GM/shear-scaling in Fig. 6b, a multi-mode (free wave) structure. The transition between the free wave vertical structure ($\sigma > 4 \pm 1$ cpd) and the mode-1 near-inertial structure ($f \leq \sigma < 2.5$ cpd) was found between $2.5 < \sigma < 4 \pm 1$ cpd (Fig. 6c). Our data did not allow more

specific determination of the transition frequency. The above mean vertical structure was confirmed from time domain analysis.

4.3. Depth-time distributions of IWB currents in summer

Above the 20 m thick tidal frictional bottom boundary layer we found near-inertial currents superimposed on tidal currents (Fig. 7a). The phase of the beat varied by 180° across layers of relatively strong stratification. Hence, inertial motions appeared in a 'mode-1' structure. The associated shear was strictly confined to the stratification (Fig. 7b). Both dominant near-inertial shear in the upper thermocline (between $-15 < z < -10$ m) and near-inertial/tidal shear in the lower thermocline (between $-25 < z < -20$ m) provided a basis of shear magnitude slowly varying with time as a result of their near-circular polarisation (Van Haren, 2000). Superposed on this slowly varying shear were weaker shear varying at time scales shorter than the inertial period, e.g. associated with $M_2 + f$. The largest shear was found between days 196–197 in the lower thermocline and between days 198–198.5 in the upper thermocline. During these periods and at these depths we found the largest amplitudes ($|U|_{iw}$) of total internal wave band currents (Fig. 7c).

In contrast with $|S|(z, t)$ being strictly confined to stratification, $|U|_{iw}(z, t)$ deviated from N(z, t) more or less following a *diurnal* migration between the two major thermoclines. Detailed inspection of Figs. 7c and 8 revealed frequently occurring quasi-random vertical phase shifts as inferred from lines of maximum current sloping backwards and forwards in the (z, t)-plane and more irregular than near-inertial motions in $|u|$. This indicated varyingly propagating

Fig. 7. Time-depth plots of various parts of currents observed in summer. In each panel stratification is presented by solid isotherms drawn every 1 °C, between 10–17 °C. (a) Total baroclinic current amplitude. Note the M_2-f beat period (~ 3.3 days) at depths above the lower thermocline, being 180° out-of-phase across the upper thermocline. Although obvious, this beat period is less pronounced than in the raw data that include the barotropic tidal current (Van Haren et al., 1999). In the baroclinic record it is due to the modification of barotropic (tidal) currents by varying viscosity associated with stratification that 'remain' in the baroclinic signal (visible in spectra in Figs. 5c, 6b; see also Maas and Van Haren, 1987). It is also partially due to the inclusion of sub-inertial motions generated at the beat frequency following non-linear tidal-inertial interactions (Van Haren et al., 2002). Here and in subsequent panels, occasionally bad current observations are above 5–8 m depth (dark red). (b) Vertical current shear magnitude. Below 25 m depth, shear is dominated at the *tidal* frequency. Above this depth it is dominated at the *inertial* frequency. (c) 'Total' non-inertial baroclinic IWB current amplitude, obtained by band pass filtering baroclinic currents between $2.5 < \sigma < 25$ cpd. About 1.5 days of data are lost at the beginning and the end of the record, due to the use of a symmetric, phase preserving filter.
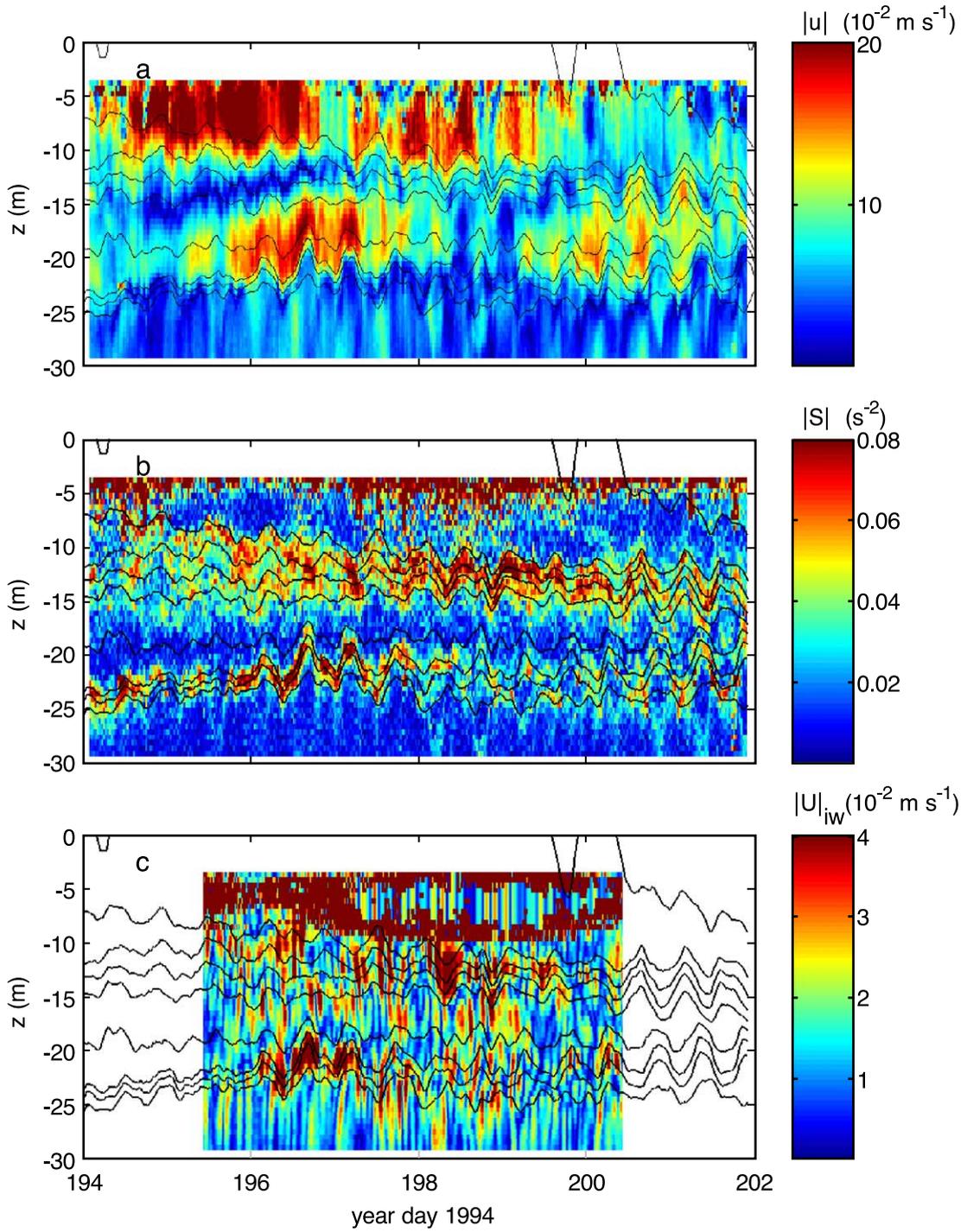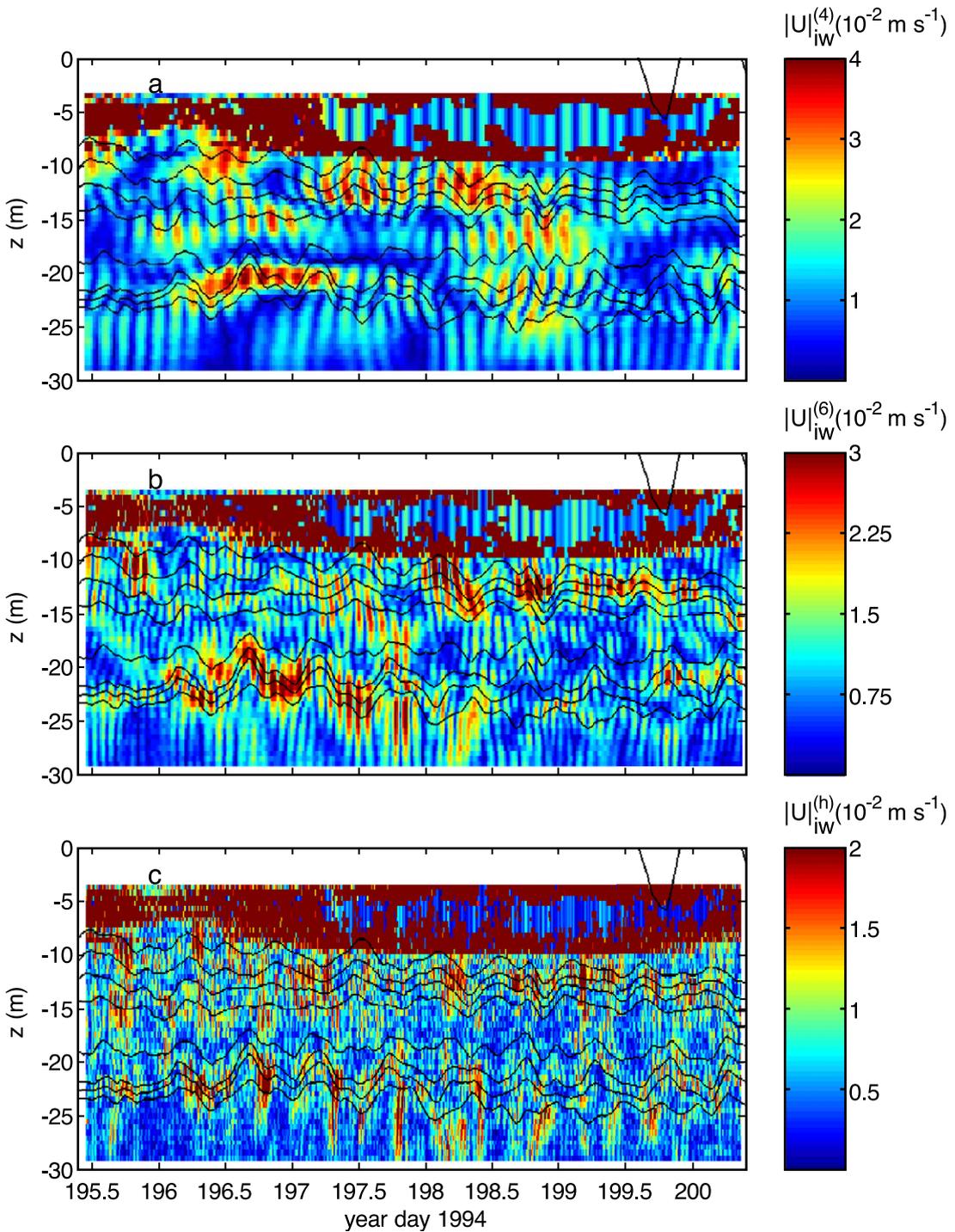
Fig. 8. Time-depth plots of magnitudes of band-pass filtered baroclinic currents from the IWB observed in summer. Stratification is presented as in Fig. 7, while the horizontal axis is shorter due to the filtering. Note different colours scaling in the panels. (a) Current amplitude of the 'fourth-diurnal' frequency band $2.5 < \sigma < 5$ cpd. (b) Current amplitude of the 'sixth-diurnal' frequency band $4.5 < \sigma < 10$ cpd. (c) Current amplitude of the 'high frequency' internal wave band $9 < \sigma < 25$ cpd.

waves. In the vertical the wavenumber was low at most frequencies, albeit changing with time. $\mathbf{U}_{iw}^{(4)}$ was primarily responsible for IWB enhancement *between* the thermoclines (Figs. 6c and 8a), where $N \gg \sigma_{M4}$. $\mathbf{U}_{iw}^{(6)}$ showed most correspondence with N and $|\mathbf{S}|$ (Figs. 7b and 8b).

Especially below the upper thermocline $\mathbf{U}_{iw}^{(4)}$ showed a typical beat period of slightly more than 2 days (Fig. 8a), which identified primary interaction frequencies such as $|2f\text{-}M_4|$ (beat period of 1.7 days) and $|(M_2 + f) - S_4|$ (2.3 days). In the near-surface part of the upper thermocline, the diurnal beat was visible. Similarly, a semidiurnal beat was visible for $\mathbf{U}_{iw}^{(h)}$, especially in the lower thermocline (Fig. 8c). All beats pointed to a coupling between IWB motions and lower frequency motions, including tidal and inertial. Note that the period of 4.5 days of filtered observations in Fig. 8 was too short to resolve the potentially dominant beat period of $|(M_2 + f) - M_4|$, which was equal to the beat period of $|M_2 - f|$.

5. Discussion

In winter in a shelf sea, atmospheric forcing was responsible for driving most of the sub-inertial kinetic energy and a non-negligible amount of energy in the IWB. Despite sufficient forcing we observed only this broad-band response to atmospheric forcing and no inertial motions. Superposed on this broad-band response were barotropic tidal motions and bounded higher tidal harmonics resulting from local non-linear interactions induced by small variations in the frictional boundary layer and topography. These higher tidal harmonics were near-deterministic as they were sharply peaked in spectral appearance. Therefore they did not represent free internal waves, which had a relatively broad spectral appearance. When stratification was enhanced through heating by the sun, this picture changed as follows.

In summer, despite weaker atmospheric kinetic energy input, we observed a narrow-band, apparent low-mode, near-inertial response following sufficient stratification to support its associated shear and slab-layer motion. Despite loss of broad-band IWB response to atmospheric forcing, energy levels increased throughout the IWB. This was also due to near-inertial motions, which fed higher frequency IWB motions after non-linear interaction with the tide. We saw a summertime IWB that was dominated at an enhanced number of interaction frequencies. Therefore the kinetic energy spectrum had a more mature and filled character around the barotropic (tidal harmonics) interaction frequencies than was observed under less stratified conditions (Fig. 2c).

As barotropic tidal energy input was the same in summer and winter, the crucial difference in observed spectra was due to the different response to external energy input through the surface. This non-tidal energy summed over the entire frequency range amounted to 25% of the total kinetic energy E_k^{tot} contents in the central North Sea. Despite the different response, this amount was, to within 5%, the same for winter (w) and summer (s),

$$\left(E_k^{tot}\right)_w \propto |\mathbf{U}|_w^2 = 0.56 \, m^2 s^{-2} \text{ and}$$

$$|\mathbf{U}|_s^2 = 0.54 \, m^2 s^{-2} \quad \cdot \quad (z = -22 \, m) \tag{6}$$

This meant that the near-inertial/IWB response to heat storage in summer was as large as the broad-band (mainly sub-inertial) response to wintertime wind stresses,

$$E_k(\text{broadband response to winter atmospheric forcing})$$

$$\cong E_k(f, M_4 - f, M_2 + f, M_4 + f, \ldots) \tag{7}$$

This implied wintertime kinetic energy input through atmospheric forcing being equivalent to summertime potential energy input by heating of the sun, because $N \approx |\mathbf{S}|$. We found such equivalence more or less by computing the dominant terms describing changes in potential energy of a water column following Van Aken (1986),

$$\frac{1}{T} \int_{January} \delta \rho_a C_D |\mathbf{W}|^3 \quad dt = 5.7 \times 10^{-3} \, Wm^{-2}$$

$$\frac{1}{T} \int_{July} -0.5 g H \overline{w' \rho'}_0 \quad dt = 4.8 \times 10^{-3} \, Wm^{-2}, \tag{8}$$

and $\delta = 0.001$ was a dimensionless efficiency parameter (Simpson and Bowers, 1981; Van Aken, 1986). In the central North Sea tidal friction is small with

respect to the terms in (8). Note that values are a factor 10 larger than in Van Aken (1986). The averaging period was T (= 1 month). Note that the relation between observed summer and winter kinetic energy and the values in (8) depends on the efficiency of transfer to available potential energy, which relies on horizontal variations in the density field created by tidal mixing (Simpson and Hunter, 1974). Validation of this relation and the efficiency parameter in (8) was beyond the scope of this paper, also because of the shortness of the data records. Qualitatively it may be stated that, as wind stress and stratification followed a seasonal cycle, so did near-inertial motions, near-inertial shear and non-linear internal waves.

6. Conclusions

Observations from 8-d records were presented from a single mooring site in the central North Sea, with focus on the construction of the internal wave spectral band under varying stratification. In addition to the lack of free internal tidal waves reported previously, it was shown that:

- Spectral observations indicated the central North Sea was sufficiently stratified year-around to support internal waves having a narrow band of frequencies larger than $f < \sigma < N \sim 4f$. CTD-density profiles showed $N \approx 10f$ in the bottom half of the water column. The discrepancy between N measured directly and inferred from spectra was due to IWB dominated by atmospheric response 'noise' or N varying on time scales shorter than inertial, preventing internal wave development.
- In summer, when $N > 10f$, motions at $f \le \sigma < 2.5$ cpd were in low vertical mode, whilst at higher IWB frequencies kinetic energy scaled with mean (mainly inertial-tidal) shear.
- In weakly stratified waters in winter, no strong near-inertial motions were observed because near-inertial mode-1 motions implied strong shear across strong stratification.
- In summer, nearly all enhanced IWB energy was at the inertial frequency. With enhanced kinetic energy at f under enhanced N (or rather shear, being better observable in weak stratification), baroclinic IWB

energy was enhanced too, in smoothed form more or less following GM. However, this enhancement was found at individual inertial-tidal interaction frequencies dominating the IWB and sloping steeper with frequency than GM, confirming recent deep-sea observations (Van Haren et al., 2002).

References

Davies, A.M., Xing, J., 2002. Processes influencing suspended sediment movement on the Malin-Hebrides shelf. Cont. Shelf Res. 22, 2081–2113.

Dronkers, J.J., 1964. Tidal Computations in Rivers and Coastal Waters. North Holland Publishing, Amsterdam, The Netherlands, 518 pp.

Fofonoff, N.P., Webster, F., 1971. Current measurements in the Western Atlantic. Phil. Trans. R. Soc. Lond. A 270, 423–436.

Garrett, C.J.R., Munk, W.H., 1972. Space-time scales of internal waves. Geophys. Fluid Dyn. 2, 225–264.

Gieskes, W.W.C., Kraay, G.W., 1984. Phytoplankton, its pigments, and primary production at a central North Sea station in May, July and September 1981. Neth. J. Sea Res. 18, 51–70.

Gill, A.E., 1982. Atmosphere-Ocean Dynamics Academic Press, Orlando, FL 662 pp.

Howarth, M.J., 1998. The effect of stratification on tidal current profiles. Cont. Shelf Res. 18, 1235–1254.

Krauss, W., 1972. On the response of a stratified ocean to wind and air pressure. D. Hyd. Z. 25, 49–61.

LeBlond, P.H., Mysak, L.A., 1978. Waves in the Ocean Elsevier, Amsterdam, 602 pp.

Maas, L.R.M., Van Haren, J.J.M., 1987. Observations on the vertical structure of tidal and inertial currents in the central North Sea. J. Mar. Res. 45, 293–318.

Mihaly, S.F., Thomson, R.E., Rabinovich, A.B., 1998. Evidence for non-linear interaction between internal waves of inertial and semidiurnal frequency. Geophys. Res. Lett. 25, 1205–1208.

Millot, C., Crépon, M., 1981. Inertial oscillations on the continental shelf of the Gulf of Lions-Observations and theory. J. Phys. Oceanogr. 11, 639–657.

Munk, W., 1981. Internal waves and small-scale processes. In: Warren, B.A., Wunsch, C. (Eds.), Evolution of Physical Oceanography. MIT Press, Cambridge, MA, pp. 264–291.

Parker, B.B. (Ed.), 1991. Tidal Hydrodynamics. John Wiley and Sons, New York, 883 pp.

Pingree, R.D., Griffiths, D.K., 1978. Tidal fronts on the shelf seas around the British Isles. J. Geophys. Res. 83, 4615–4622.

Pingree, R.D., Maddock, L., 1978. The M_4 tide in the English Channel derived from a non-linear numerical model of the M_2 tide. Deep-Sea Res. 26, 53–68.

Platzman, G.W., 1964. An exact integral of complete spectral equations for unsteady one-dimensional flow. Tellus 16, 422–431.

Pollard, R.T., Millard Jr., R.C., 1970. Comparison between observed and simulated wind-generated inertial oscillations. Deep-Sea Res. 17, 813–821.

Pollard, R.T., Rhines, P.B., Thompson, R.O.R.Y., 1973. The deepening of the wind-mixed layer. Geophys. Fluid Dyn. 3, 381–404.

Pond, J.S., Pickard, G.L., 1986. Introductory Dynamical Oceanography, 2nd ed. Pergamon Press, Oxford, 329 pp.

Simpson, J.H., Bowers, D., 1981. Models of stratification and frontal movement in shelf seas. Deep-Sea Res. 28, 727–738.

Simpson, J.H., Hunter, J.R., 1974. Fronts in the Irish Sea. Nature 250, 404–406.

Van Aken, H.M., 1986. The onset of seasonal stratification in shelf seas due to differential advection in the presence of a salinity gradient. Cont. Shelf Res. 5, 475–485.

Van Haren, J.J.M., Maas, L.R.M., 1987. Temperature and current fluctuations due to tidal advection of a front. Neth. J. Sea Res. 21, 79–94.

Van Haren, H., 2000. Properties of vertical current shear across stratification in the North Sea. J. Mar. Res. 58, 465–491.

Van Haren, H., 2001. Estimates of sea level, waves and winds from bottom-mounted ADCP in a shelf sea. J. Sea Res. 45, 1–14.

Van Haren, H., Maas, L., Zimmerman, J.T.F., Ridderinkhof, H., Malschaert, H., 1999. Strong inertial currents and marginal internal wave stability in the central North Sea. Geophys. Res. Lett. 26, 2993–2996.

Van Haren, H., Maas, L., Van Aken, H., 2002. On the nature of internal wave spectra near a continental slope. Geophys. Res. Lett. 29 (12) (10.1029/2001GL014341).

Van Raaphorst, W., Malschaert, H., Van Haren, H., 1998. Tidal resuspension and deposition of particulate matter in the oyster grounds, North Sea. J. Mar. Res. 56, 257–291.